

Long-term Hard X-ray Monitoring of 2S 0114+65 with INTEGRAL/IBIS

Wei Wang^{*}

National Astronomical Observatories, Chinese Academy of Sciences, Beijing 100012, China

20 June 2018

ABSTRACT

We present the results of the long-term hard X-ray monitoring of the high mass X-ray binary 2S 0114+65 with INTEGRAL/IBIS from 2003 to 2008. 2S 0114+65 is a variable hard X-ray source with X-ray luminosities of $10^{35} - 4 \times 10^{36}$ erg s⁻¹ from 20 – 100 keV due to accretion rate changes in different orbital phases. In several observations when 2S 0114+65 was bright, we found a pulse period evolution of ~ 2.67 hour to 2.63 hour from 2003 – 2008, with a spin-up rate of the neutron star $\sim 1.09 \times 10^{-6}$ s s⁻¹. Compared with the previous reported spin-up rate, the spin-up rate of the neutron star in 2S 0114+65 is accelerating. The spectral properties of 2S 0114+65 in the band of 18 – 100 keV which changed with the orbital phases, generally could be described with a power-law model with a high energy exponential cutoff. The variation of the power-law photon index over orbital phase anticorrelates with hard X-ray flux, and the variation of E_{cut} has a positive correlation with the hard X-ray flux, implying that the harder spectrum at the maximum of the light curve. The variations of spectral properties over orbital phase suggested 2S 0114+65 as a highly obscured binary system. In some observational revolutions, hard X-ray tails above 70 keV are detected. We study the characteristics of the hard X-ray tails combining JEM-X and IBIS data in the energy range of 3 – 100 keV. The 3 – 100 keV spectra of 2S 0114+65 are generally fitted by an absorbed power-law model with high energy cutoff. We discover that the hard X-ray tails are only detected when column density is very low. Thus, high column density leads to disappearance of the hard X-ray tails in this wind-fed neutron star accretion binary. Our results would help to understand the origin, evolution and properties of this peculiar class of super-slow pulsation neutron stars in high mass X-ray binaries.

Key words: stars: individual (2S 0114+65) – stars: neutron – stars : binaries : close – X-rays: binaries.

1 INTRODUCTION

The high mass X-ray binary 2S 0114+65 is an unusual system, which shows properties consistent with both Be and supergiant X-ray binaries, with significant temporal and spectral variability over a wide range of time scales (Crampton et al. 1985). A type B1a supergiant optical counterpart (LS I+65010) at a distance of ~ 7.2 kpc was identified (Reig et al. 1996). 2S 0114+65 has an orbital period of ~ 11.59 day (Crampton et al. 1985; Corbet et al. 1999; Wen et al. 2006; Grundstrom et al. 2007). A superorbital modulation at ~ 30.7 day was also reported from the analysis of 8.5 years of RXTE/ASM data (Farrell et al. 2006). The low X-ray luminosity of $\sim 10^{36}$ erg s⁻¹ (in the 3– 20 keV band,

Hall et al. 2000) implies that spherical accretion takes place via the stellar wind of the donor star in 2S 0114+65 (Li & van den Huevel 1999). It should be noted that the He II 4686 Å line (a common signature of the presence of an accretion disc) has been observed in some occasions but was very weak (Aab et al. 1983, Crampton et al. 1985), possibly linked to the presence of a small transient accretion disc.

The X-ray source 2S 0114+65 consists of an wind-fed accretion neutron star with its pulse period first measured at ~ 2.78 hr by Finley et al. (1992). Hall et al. (2000) derived a period of ~ 2.73 hr, and found a spin-up rate of $\sim 6.2 \times 10^{-7}$ s s⁻¹ for the neutron star in 2S 0114+65 over ~ 11 yr. Using the INTEGRAL/IBIS data, Bonning & Falanga (2005) obtained a spin period of ~ 2.67 hr, and a spin-up rate of $\sim 8.9 \times 10^{-7}$ s s⁻¹ from 1996 to 2004. Farrell et al. (2008) analyzed pointed observation data of RXTE around

^{*} E-mail: wangwei@bao.ac.cn

early 2006 to derive a spin period of ~ 2.65 hr. From 2004 to 2006, the spin-up rate of 2S 0114+65 was $\sim 1.6 \times 10^{-6} \text{ s s}^{-1}$ if we compare the results by INTEGRAL (Bonning & Falanga 2005) and RXTE (Farrell et al. 2008). Then the spin-up rate seems to be accelerating in recent years though the pulsed period was derived from different instruments. The reported long spin period in 2S 0114+65 makes it one of the slowest X-ray pulsars. Many theoretical models have been suggested to explain this long period pulsation (Hall et al. 2000; Li & van den Heuvel 1999; and references therein). Li & van den Heuvel (1999) suggested the magnetar origin for the neutron star in 2S 0114+65 to explain the slow pulsation. At present, the magnetic field of the neutron star in 2S 0114+65 has not been determined. The possible electron cyclotron resonant absorption features at ~ 22 keV and 44 keV was reported by Bonning & Falanga (2005), implying a magnetic field of $\sim 2.5 \times 10^{12}$ G.

2S 0114+65 as an accretion neutron star system has the typical X-ray spectrum (i.e., 1 – 50 keV) fitted with an absorbed power-law model with the high energy exponential cut-off (Farrell et al. 2008; Masetti et al. 2006; Hall et al. 2000). Recently, den Hartog et al. (2006) found the high energy tail above 70 keV in 2S 0114+65 using the INTEGRAL/IBIS data. The origin of the hard X-ray tail in 2S 0114+65 is unclear. In addition, we need to study the hard X-ray spectra up to 100 keV to confirm the existence of the hard X-ray tails in 2S 0114+65.

In this paper, we present our results of long-term high energy monitoring of 2S 0114+65 up to ~ 100 keV with INTEGRAL/IBIS observations from 2003 to 2008. Our scientific studies mainly aim to discover the different hard X-ray properties of 2S 0114+65 in different accretion states, search for the hard X-ray tails and possible electron cyclotron absorption feature in the spectra and derive the pulse period of 2S 0114+65 in different time intervals to probe the spin-up rate of the neutron star from 2003 to 2008. Observations of IBIS and science data analysis were described in §2. In §3, we show the timing analysis and results of spin period evolution. The spectral properties in different accretion states/orbital phases and searching for hard X-ray tails and possible cyclotron absorption features were presented in §4. Summary and discussions of the results were given in the last section.

2 OBSERVATIONS AND DATA ANALYSIS

The INTERNATIONAL Gamma-Ray Astrophysics Laboratory (INTEGRAL, Winkler et al. 2003) is ESA's currently operational space-based hard X-ray/soft gamma-ray telescope. There are two main instruments aboard INTEGRAL, the imager IBIS (Ubertini et al. 2003) and the spectrometer SPI (Vedrenne et al. 2003), supplemented by two X-ray monitors JEM-X (Lund et al. 2003) and an optical monitor OMC (Mas-Hesse et al. 2003). All four instruments are co-aligned, allowing simultaneous observations in a wide energy range. SPI has a lower sensitivity than IBIS for weak source below 100 keV, and detection of weak point sources is not so significant for spectral studies. Here we use the data collected with the low-energy array called IBIS-ISGRI (INTEGRAL Soft Gamma-Ray Imager) which consists of a pixellated 128×128 CdTe solid-state detector that views the sky through a coded

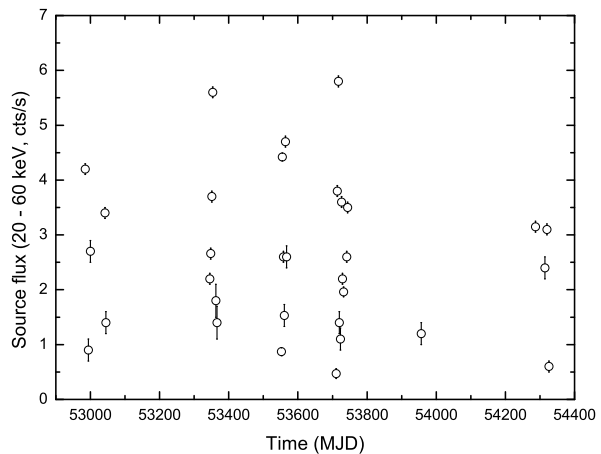


Figure 1. The light curve of the high massive X-ray binary 2S 0114+65 binning at ~ 3 days in the energy range of 20– 60 keV observed by IBIS from 2003 Dec to 2008 May.

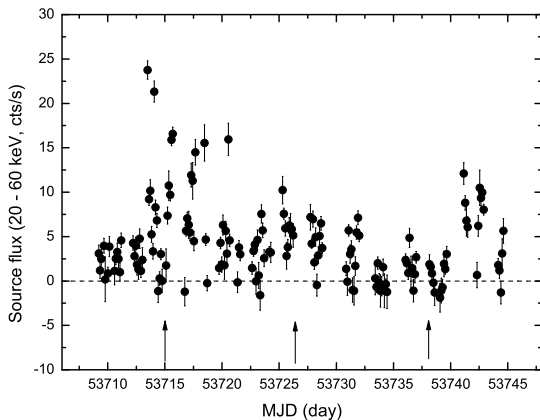


Figure 2. Hard X-ray light curve of 2S 0114+65 observed by INTEGRAL/IBIS from the revolutions 384 – 395 with 0.15 day binning. For a comparison, we also show the maximum flux from 1.5 – 12 keV based on the RXTE/ASM data which is indicated with the arrows.

aperture mask (Lebrun et al. 2003). IBIS/ISGRI has a $12'$ (FWHM) angular resolution and arcmin source location accuracy in the energy band of 15 – 200 keV. JEM-X collects the lower energy photons from 3 – 35 keV. Since JEM-X has a small field of view (like requiring off-axis angle $< 5^\circ$) and a relatively low sensitivity because of small detector area (Lund et al. 2003), the source 2S 0114+65 was only significantly detected in a few time intervals. We use the JEM-X data combined with IBIS observations in some special time intervals to constrain the hard X-ray tails from the broadband spectra.

The high mass X-ray binary 2S 0114+65 was observed frequently during the INTEGRAL surveys of the Cassiopeia

Table 1. INTEGRAL/IBIS observations of the field around 2S 0114+65. The time intervals of observations in the revolution number and the corresponding dates, the corrected on-source exposure time, mean off-axis angle on the source are listed. And mean count rate and the detection significance level value in the energy range of 20 – 60 keV were also shown.

Rev. Num.	Date	On-source time (ks)	off-axis angle	Mean count rate s ⁻¹	Detection level
142	2003 Dec 12–14	99	7.9°	4.1±0.1	33σ
143	2003 Dec 15–17	94	7.7°	< 0.6	< 5σ
144	2003 Dec 18 – 20	90	7.8°	< 0.7	< 5σ
145	2003 Dec 21 –23	93	9.8°	0.9 ± 0.2	5σ
146	2003 Dec 24 –26	58	6.5°	< 0.7	< 5σ
147	2003 Dec 27 –38	92	9.7°	2.9 ± 0.2	15σ
148	2003 Dec 30 – 2004 Jan 01	91	7.9°	< 0.6	< 5σ
161	2004 Feb 7 – 9	75	9.7°	3.4 ± 0.1	33σ
162	2004 Feb 10 – 12	78	9.8°	1.4 ± 0.2	7σ
238	2004 Sep 24 – 26	198	1.8°	< 0.4	< 5σ
262	2004 Dec 6 – 7	63	2.1°	2.2±0.1	19.6σ
263	2004 Dec 8 – 10	76	1.9°	2.66±0.09	27σ
264	2004 Dec 11 – 13	97	8.5°	3.7±0.1	35σ
265	2004 Dec 14 – 16	103	8.7°	5.6±0.1	48σ
266	2004 Dec 17 – 19	86	9.1°	< 0.7	< 5σ
268	2004 Dec 20 – 22	45	8.9°	1.8 ± 0.3	6σ
269	2004 Dec 23 – 25	81	8.8°	1.4 ± 0.3	5σ
331	2005 June 29 – July 2	190	3.1°	0.87 ± 0.07	12.9σ
332	2005 Jul 2 – 5	173	3.4°	4.42 ± 0.07	61.4σ
333	2005 Jul 5 – 7	206	3.3°	2.60 ± 0.06	40.5σ
334	2005 Jul 8 – 10	60	4.3°	1.53 ± 0.13	11.3σ
335	2005 Jul 11 – 13	170	4.6°	4.69 ± 0.08	59.1σ
336	2005 Jul 14 – 16	104	5.3°	2.56 ± 0.17	15.3σ
384	2005 Dec 5 – 7	99	8.1°	0.47 ± 0.09	5σ
385	2005 Dec 8 – 10	98	9.3°	3.9 ± 0.1	37σ
386	2005 Dec 11 – 13	101	9.0°	5.8±0.1	55σ
387	2005 Dec 14 – 16	90	8.7°	1.4 ± 0.2	7σ
388	2005 Dec 17 – 19	93	8.3°	1.1 ± 0.2	5σ
389	2005 Dec 20 – 22	108	7.9°	3.6 ± 0.1	35σ
390	2005 Dec 23 – 25	117	7.7°	2.2±0.1	23σ
391	2005 Dec 26 – 28	93	8.4°	1.96±0.09	19σ
392	2005 Dec 29 – 31	105	8.6°	< 0.3	< 5σ
393	2006 Jan 1 – 3	88	8.5°	< 0.4	< 5σ
394	2006 Jan 4 – 6	102	8.0°	2.6 ± 0.1	25σ
395	2006 Jan 7 – 9	98	7.8°	3.5 ± 0.1	36σ
454	2006 Jul 4 – 6	208	1.3°	< 0.4	< 5σ
466	2006 Aug 7 – 9	78	8.9°	1.2±0.2	7σ
528	2007 Feb 8 – 10	196	1.5°	< 0.4	< 5σ
664	2008 Mar 21 – 23	95	1.6°	3.15±0.10	30σ
667	2008 Mar 30 – Apr 01	46	1.4°	< 0.6	< 5σ
668	2008 Apr 2 – 4	44	1.4°	< 0.6	< 5σ
669	2008 Apr 5 – 7	44	1.1°	< 0.5	< 5σ
670	2008 Apr 8 – 10	47	0.9°	< 0.5	< 5σ
673	2008 Apr 17 – 19	50	0.9°	2.37 ± 0.14	16.5σ
675	2008 Apr 23 – 25	109	0.7°	3.09 ± 0.09	39.2σ
677	2008 Apr 29 – May 1	96	0.8°	0.60 ± 0.09	6.3σ

region. In this work, we use the available archival data for the IBIS observations where 2S 0114+65 was within ~ 10 degrees of the pointing direction. In Table 1, we summarize the INTEGRAL/IBIS observations in our analysis, including the revolution numbers, corrected exposure time and off-axis angle on the source for each revolution. The archival data used in our work are available from the INTEGRAL Science Data Center (ISDC).

The analysis was done with the standard INTEGRAL off-line scientific analysis (OSA, Goldwurn et al. 2003) software, ver. 7.0. Individual pointings processed with OSA 7.0 were mosaicked to create sky images according to the methods and processes described in Bird et al (2007). We used the 20 – 60 keV band for source detection and to quote source fluxes for each revolution (see Table 1). In most revolutions, 2S 0114+65 was detected significantly with IBIS, while for some orbit phases, the source was not detected (the detection significance level was lower than 5σ), then only the upper limits of the count rates were given in Table 1.

In Figure 1, the light curve of 2S 0114+65 from 2003

December to 2006 August in the energy range of 20 – 60 keV detected by IBIS was displayed. 2S 0114+65 is a variable source whose mean hard X-ray flux in each revolution detected by IBIS varied from ~ 0.4 cts/s to ~ 6 cts/s in the range of 20 – 60 keV. This X-ray variability could be due to different accretion states or accretion in the different orbit phases if the orbit is eccentric. In this paper we classify the light curve into two accretion states: quiescent states with average flux below ~ 1 cts/s or non-detection in one revolution observations; and active states. For these different accretion states, 2S 0114+65 would have different spectral properties which will be studied in §4.

3 TIMING ANALYSIS AND SPIN PERIOD EVOLUTION OF 2S 0114+65

The high massive X-ray binary 2S 0114+65 has an orbital period of ~ 11.59 days according to the regular soft X-ray observations by RXTE/ASM (Corbet et al. 1999; Farrell

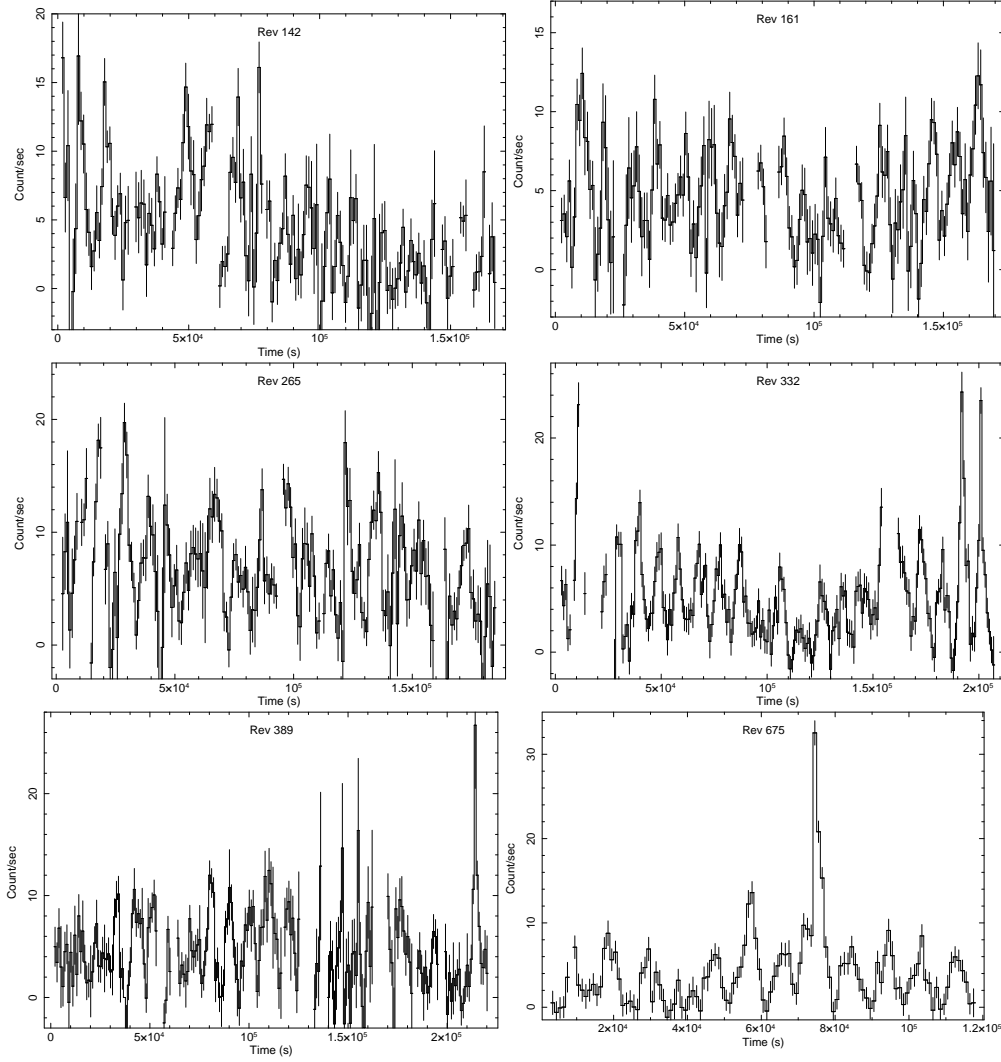


Figure 3. IBIS background subtracted hard X-ray light curves of 2S 0114+65 in the energy band of 20 – 60 keV for six different time intervals: Rev 142 (2003 Dec), 161 (2004 Feb), 265 (2004 Dec), 332 (2005 July), 389 (2005 Dec) and 675 (2008 April).

et al. 2008). Hard X-ray observations by IBIS/ISGRI have shown that 2S 0114+65 is a variable source. Its variability may also be related to the orbital modulation. IBIS had continuous observations of 2S 0114+65 from 2005 Dec 5 – 2006 Jan 9. This observational time scale covered about 3 orbit periods (Figure 2). The hard X-ray light curves from 20 – 60 keV of 2S 0114+65 show no obvious orbital modulation. For a comparison, we also show the epochs of the maximum flux from 1.5 – 12 keV derived by RXTE/ASM in the same time interval from MJD 53700 – 53750, as indicated with the arrows.

Our IBIS observations of the X-ray pulsar 2S 0114+65 covered near 5 years, so it is the good way for us to derive the spin period evolution of 2S 0114+65 from 2003 to 2008 using the present data.

3.1 Spin period evolution

To search for the pulsation period and the spin evolution of 2S 0114+65, we use the observational data in which 2S 0114+65 has a higher detection significant level (e.g., $> 30\sigma$,

see Table 1). Then we select the databases for six time intervals covering nearly 5 years: 2003 Dec 12 – 14 (Rev 142); 2004 Feb 7 – 9 (Rev 161); 2004 Dec 14 – 16 (Rev 265); 2005 Jul 2 – 5 (Rev 332); 2005 Dec 20 – 22 (Rev 389) and 2008 Apr 23 – 25 (Rev 675). The minimum time bins in analysis are taken as ~ 200 s for each dataset. The hard X-ray light curves in the energy band of 20 – 60 keV obtained by IBIS/ISGRI in six time intervals are presented in Figure 3 and the barycentric corrections were also made. The X-ray light curves in Fig. 3 have been re-binned to 1000 s for clarity. We apply FFT on each of the six light curves to search for the modulation period signals. The power spectra for each light curve are displayed in Figure 4. Significant modulation period signals around ~ 9500 – 9600 s are found for all light curves.

According to the position of peak signals in the power spectra (Figure 4), we use the pulse-folding technique to derive the pulse period values of 2S 0114+65 for the six time intervals: $P = 9612 \pm 20$ s for Rev 142; $P = 9600 \pm 20$ s for Rev 161; $P = 9570 \pm 20$ s for Rev 265; $P = 9555 \pm 15$ s for Rev 332; $P = 9520 \pm 20$ s for Rev 389; and $P = 9475 \pm 25$ s for Rev

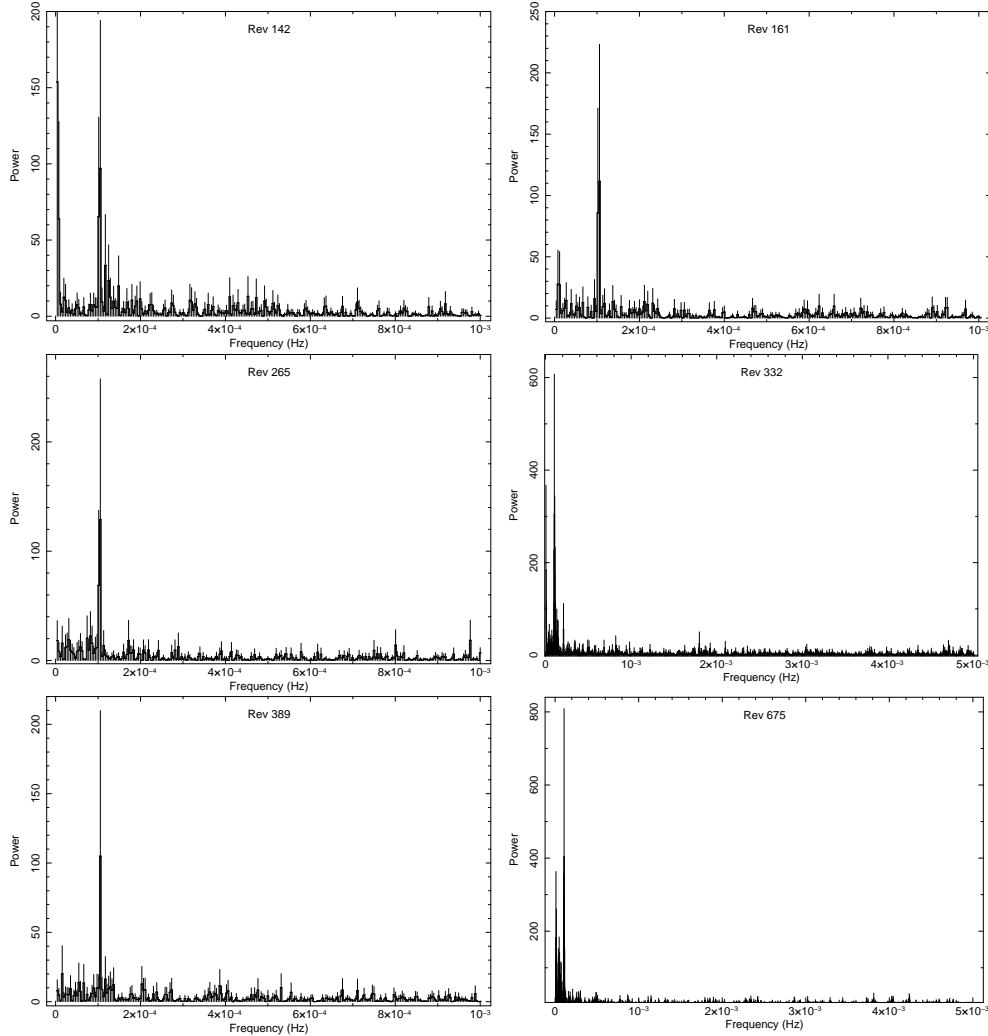


Figure 4. Power spectra of hard X-ray light curves of 2S 0114+65 for six different time intervals in Fig. 3: Rev 142 (2003 Dec), 161 (2004 Feb), 265 (2004 Dec), 332 (2005 July), 389 (2005 Dec) and 675 (2008 April).

675. Figure 5 shows the light curves of 2S 0114+65 folded with the derived pulse period in six time intervals. The pulse light curves show the single main peak feature. The pulse fraction defined as the ratio of the pulse maximum minus the minimum to the maximum can also be estimated for each pulse light curve. We found the pulse fractions of $\sim (95 \pm 5)\%$ for Rev 142, $\sim (89 \pm 8)\%$ for Rev 161, $\sim (88 \pm 7)\%$ for Rev 265, $\sim (86 \pm 4)\%$ for Rev 332, $\sim (85 \pm 9)\%$ for Rev 389, $\sim (91 \pm 6)\%$ for Rev 675.

The obtained pulse period values of 2S 0114+65 suggested that the X-ray pulsar in 2S 0114+65 is still spinning up. Figure 6 displayed the spin history of 2S 0114+65 from different measurements. In particular, Finley et al. (1992) derived a spin period of ~ 2.78 hr, and nine years later, Hall et al. (2000) found a pulse period of ~ 2.73 hr. More recently, Bonning & Flanga (2005) obtained a pulse period of ~ 2.67 hr using IBIS observations, and Farrell et al. (2008) got a pulse period of ~ 2.65 hr using RXTE data. From their measurements in different time intervals, we obtain a history of spin-up rates for the X-ray pulsars in 2S 0114+65: $\sim 6.2 \times 10^{-7} \text{ s s}^{-1}$ from 1986 – 1996; $\sim 8.9 \times 10^{-7} \text{ s s}^{-1}$ from 1996 to 2004; $\sim 1.6 \times 10^{-6} \text{ s s}^{-1}$ from 2004 to 2006.

Figure 6 also shows six data points using our IBIS observations from 2003 Dec to 2008 May. From our IBIS measurements in six time intervals, we can find a spin-up rate of $\sim (1.09 \pm 0.13) \times 10^{-6} \text{ s s}^{-1}$ from 2003 to 2008. Therefore, the spin period of the neutron star in 2S 0114+65 was decreasing, and the spin-up rate was really accelerating in the past thirty years.

4 SPECTRAL PROPERTIES IN HARD X-RAYS

Hard X-ray spectral properties (above 15 keV) of 2S 0114+65 have not been studied in details before. From our analysis of the five years of hard X-ray monitoring data by INTEGRAL/IBIS, we study the properties of 2S 0114+65 up to 200 keV. 2S 0114+65 is a highly variable X-ray source due to accretion variability and different orbital phases. We then study the hard X-ray spectral properties of 2S 0114+65 in different accretion states and orbital phases. In particular, we will try to search for the hard X-ray tails and possible cyclotron absorption line features around 22 keV and 44 keV

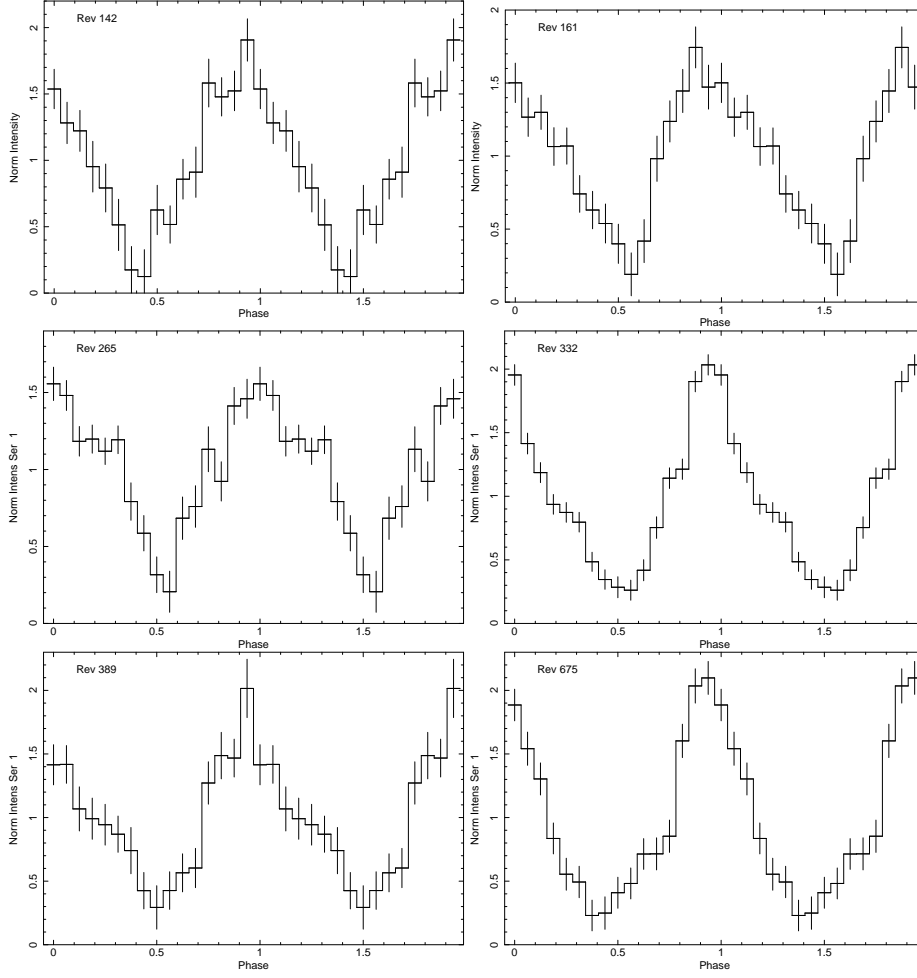


Figure 5. The IBIS/ISGR1 background subtracted light curves (20 – 60 keV) of 2S 0114+65 folded at a pulsation period for six different time intervals: Rev 142 ($P = 9612$ s), 161 ($P = 9600$ s), 265 ($P = 9570$ s), 332 ($P = 9555$ s), 389 ($P = 9520$ s), 675 ($P = 9475$ s). The pulse profiles are repeated once for clarity.

in the hard X-ray spectra. This will help us to understand the formation and evolution of this X-ray source system.

From Table 1 and Figure 1, the X-ray binary 2S 0114+65 has variable hard X-ray fluxes during the hard X-ray monitoring with IBIS from 2003 – 2008. We would show the spectral properties of 2S 0114+65 in different accretion states as defined in §2, namely active states and quiescent states. The spectral extractions for the observations of each revolution were carried out. The spectral analysis software package used is XSPEC 12.4.0x.

Spectral properties of 2S 0114+65 could be variable in different accretion rates, then we first use a simple model like a single power-law model to fit all the spectra, which show the changes of the spectra properties for comparison. In Table 2, we show the spectral properties of 2S 0114+65 in both active states and quiescent states. In the quiescent cases, we study the spectral properties in four revolutions (Rev. 145, 331, 384, 677) when the IBIS rate is below ~ 1 cts/s in Table 1. In active states, we carry out spectral analysis on the source in the revolution when 2S 0114+65 was detected with the significance levels higher than $\sim 30\sigma$ in Table 1. Since we also want to check the possible cyclotron absorption features around 22 keV and 44 keV reported by

Bonning & Falanga (2005) who used the IBIS data in Rev. 262 and 263. Then in the active case, we show the spectral properties of 2S 0114+65 for 15 revolutions in Table 2. To estimate the X-ray luminosity, we have assumed a source distance of 7.2 kpc for 2S 0114+65 throughout the paper (Reig et al. 1996).

4.1 Spectral properties in different states

4.1.1 active states

During the 5 years of hard X-ray monitoring, the high mass X-ray binary 2S 0114+65 may undergo active states in most of the time (see Fig. 1). We will derive the hard X-ray spectral information for 2S 0114+65 with the data of each revolution in active states, so that the variations of the spectral properties with time can be presented. In this subsection, we show the spectral properties of 2S 0114+65 in active states when the source was detected by IBIS with the significance levels $> 30\sigma$, which includes 13 revolutions (see Table 1). In addition, two revolutions 262 and 263 (detection significance levels are 20σ and 27σ respectively) are also included to check the possible absorption features around 44 keV reported by Bonning & Falanga (2005).

Table 2. Spectral properties of 2S 0114+65 in different accretion states and datasets (for observations in each revolution). All spectra are fitted with a single power law model for the comparison. The hard X-ray fluxes and luminosities in the range of 20 – 100 keV for the active states and 20 – 50 keV for quiescent states in model fits were also given.

Rev. Num.	Γ	Flux (10^{-10} erg cm $^{-2}$ s $^{-1}$)	L_x (erg s $^{-1}$)	reduced χ^2
The active states				
142	2.5 ± 0.1	3.0 ± 0.3	2.1×10^{36}	1.261(28d.o.f.)
161	2.8 ± 0.1	2.3 ± 0.4	1.5×10^{36}	1.252(25d.o.f.)
262	2.6 ± 0.2	1.6 ± 0.3	1.0×10^{36}	0.845(26d.o.f.)
263	2.7 ± 0.1	1.9 ± 0.3	1.2×10^{35}	1.177(26d.o.f.)
264	2.7 ± 0.1	2.5 ± 0.4	1.7×10^{36}	0.796(24d.o.f.)
265	2.6 ± 0.1	3.9 ± 0.3	2.7×10^{36}	1.352(27d.o.f.)
332	2.7 ± 0.1	3.0 ± 0.2	2.1×10^{36}	1.630(28d.o.f.)
333	2.7 ± 0.1	1.8 ± 0.2	1.1×10^{36}	1.951(28d.o.f.)
335	2.6 ± 0.1	3.3 ± 0.3	2.3×10^{36}	1.562(28d.o.f.)
385	2.7 ± 0.1	2.6 ± 0.3	1.7×10^{36}	0.973(27d.o.f.)
386	2.6 ± 0.1	4.1 ± 0.3	2.8×10^{36}	1.490(29d.o.f.)
389	2.8 ± 0.1	2.4 ± 0.3	1.5×10^{36}	1.052(29d.o.f.)
395	2.6 ± 0.1	2.4 ± 0.3	1.5×10^{36}	0.986(29d.o.f.)
664	2.8 ± 0.1	2.4 ± 0.3	1.5×10^{36}	0.956(28d.o.f.)
675	2.7 ± 0.1	2.6 ± 0.3	1.7×10^{36}	1.356(28d.o.f.)
The quiescent states				
145	2.7 ± 0.6	0.47 ± 0.11	2.9×10^{35}	0.689(5d.o.f.)
331	3.1 ± 0.3	0.51 ± 0.09	3.1×10^{35}	1.52(4d.o.f.)
384	2.6 ± 0.7	0.19 ± 0.07	1.2×10^{35}	1.21(3d.o.f.)
677	3.2 ± 0.6	0.29 ± 0.09	1.7×10^{35}	0.953(4d.o.f.)

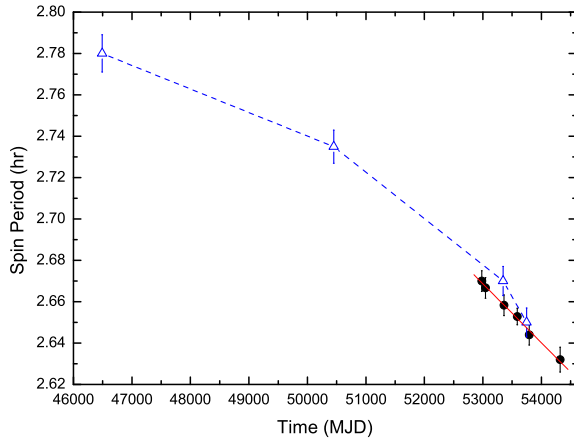


Figure 6. Spin evolution history of 2S 0114+65 from different observations. The filled circles are from this work. The open triangles are from Finley et al. (1992), Hall et al. (2000), Bonning & Flanga (2005) and Farrell et al. (2008). The dashed lines show the spin-up rates in different time intervals. The solid line presents the best fitting rate of $\sim (1.09 \pm 0.13) \times 10^{-6}$ s s $^{-1}$ from 2003 – 2008 only using our IBIS data. See details in the text.

We fit the spectra with the same model – a single power-law model. In Table 2, the detailed fitted spectral parameters for each observational revolution are presented together for the comparison. In Figure 7, we display the IBIS-ISGRI spectra of 2S 0114+65 in the active states from nine observations (as examples): Rev 161; Rev 262; Rev 263; Rev 264; Rev 265; Rev 385; Rev 386; Rev 389 and Rev 395. The spectra in the other revolutions will be shown in the following sections, so they are not repeated here.

The spectrum of the source 2S 0114+65 has been studied up to 100 keV. But 2S 0114+65 is very weak above 100 keV, and is only marginally detected in some cases (like very bright, or possible existence of high energy tails). Then the data points in the spectra of 2S 0114+65 generally show only upper limits above 100 keV. We present only a few data points above 100 keV to show the high energy behavior (no detection or possible tails) of 2S 0114+65 (see examples in Fig. 7). In Table 2, we show the hard X-ray fluxes and derived X-ray luminosity in the range of 20 – 100 keV. In active states, 2S 0114+65 has a hard X-ray luminosity in the range of $(1 - 3) \times 10^{36}$ erg s $^{-1}$ from 20 – 100 keV.

The single power-law model gives the photon index range of 2.5 – 2.8 implying moderate spectral variations in active states. The given reduced χ^2 in the power-law fittings is generally around 1, but in some revolutions it is significantly higher than 1 (see Table 2). So the simple power-law model would be unsuitable for the spectra in these revolutions. In the **Appendix**, we present an extended table to display spectral parameters for all revolutions shown in Table 2 fitted with the different models like a thermal bremsstrahlung model, a power-law model with a high energy exponential cut-off (hereafter *pow*high*) or the bremsstrahlung model plus a power-law model (for the possible hard X-ray tail case). This extended table could help the readers to justify which model may be more acceptable for each spectrum.

In active states, 2S 0114+65 was detected in hard X-rays by IBIS with a high significance level of above 30σ , which may help us to search for the possible cyclotron absorption lines around 22 keV and 44 keV reported by Bonning & Falanga (2005). Bonning & Falanga (2005) found possible absorption feature around 44 keV used the IBIS data during observations in Revs. 262 and 263. We also derived the spectrum of 2S 0114+65 in Revs. 262 and 263 but with the different energy band binning (see Fig. 7).

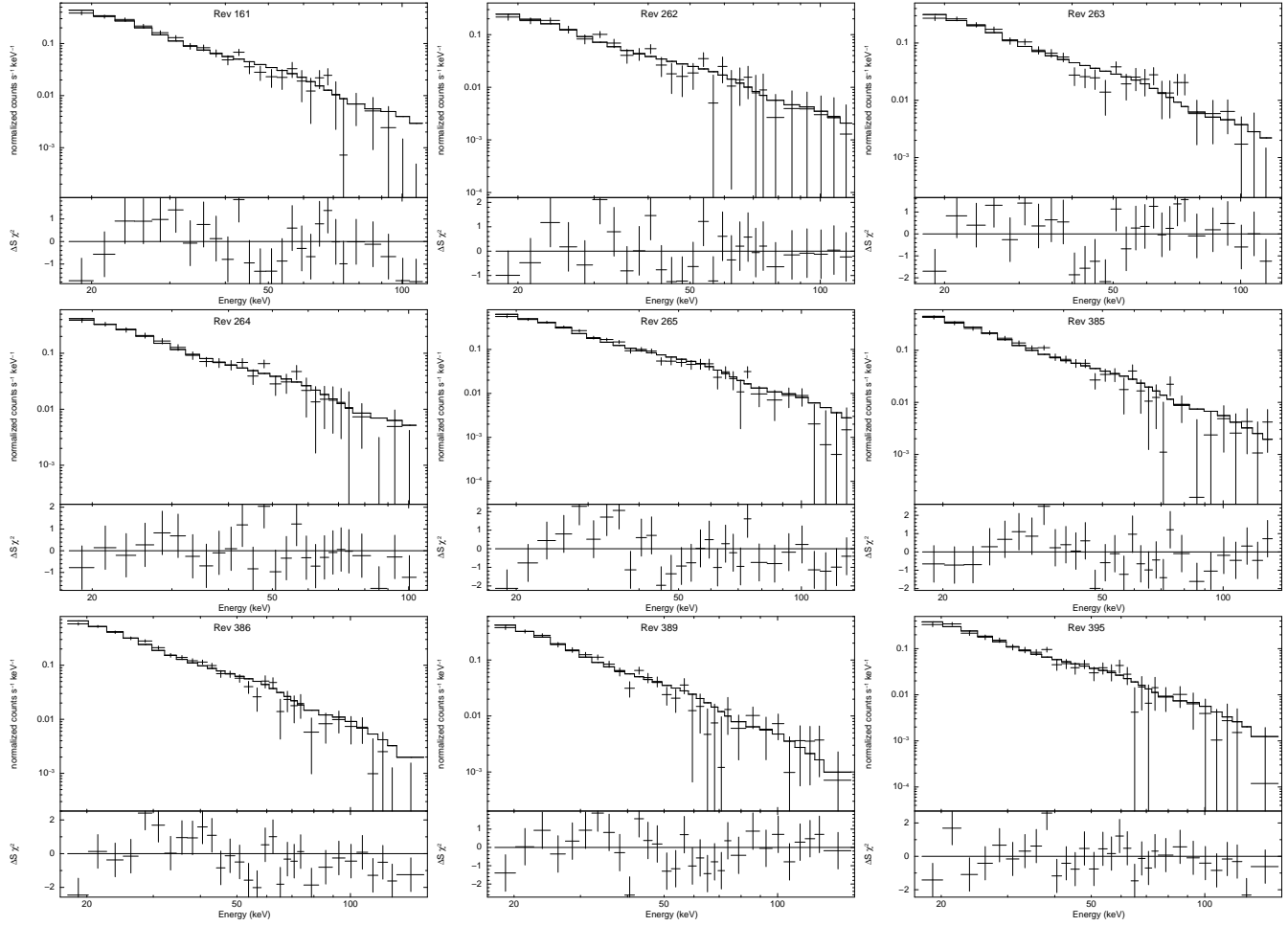


Figure 7. The hard X-ray spectra of 2S 0114+65 obtained by INTEGRAL/IBIS during the observational revolutions in the active states: 161, 262, 263, 264, 265, 385, 386, 389 and 395. All spectra are fitted with a single power-law model for comparison. The spectral properties of 2S 0114+65 evolved in the different times from our observations. See details of the fitting parameters in Table 2 and the text.

From residuals after continuum fitting, the absorption feature around 44 keV is not obvious in Rev 262, but might still exist in Rev 263. In the other seven spectra in active states presented in Fig. 7, the possible absorption feature around 44 keV was only hinted in Rev 265. In addition, possible features were also found around 54 keV in Rev 385 and around 40 keV in Rev 389. So we cannot confirm the possible cyclotron absorption features around 22 keV and 44 keV. These possible features in residuals may be induced by the flux fluctuations derived by the IBIS detectors, possibly due to effects of detector response and calibration uncertainties. However, we do not exclude the possible existence of the cyclotron absorption line around 22 keV in 2S 0114+65, because production of electron cyclotron absorption lines may depend on the accretion geometry and the relativistic cyclotron absorption line energy would have non-harmonic line spacing (Araya & Harding 1999) and fundamental line energy also changes in different observations (depending on luminosity and other relevant effects, see Klochov et al. 2008; Araya & Harding 2000).

4.1.2 quiescent states

During the IBIS/ISGRi hard X-ray monitoring of the high mass X-ray binary 2S 0114+65 from 2003 – 2006, the source 2S 0114+65 was not detected in some time intervals, or was detected with a low significance level with a mean count rate of $< 1 \text{ cts s}^{-1}$. During these time intervals, we have explained that 2S 0114+65 was undergoing the quiescent states.

From Table 2, 2S 0114+65 was detected above 5σ for four revolutions in the quiescent states. The four spectra in these revolutions are presented in Fig. 8. In the quiescent states, 2S 0114+65 cannot be detected significantly above 50 keV, and only a few data points can be used in the spectral fitting. We also use a single power-law model to fit all spectra, and spectral properties are shown in Table 2. The flux and luminosity are given only in the range of 20 – 50 keV. In quiescence, X-ray luminosity from 20 – 50 keV is around $(2 - 5) \times 10^{35} \text{ erg s}^{-1}$. The photon indexes distribute from 2.6 – 3.2 with larger error bars, so the hard X-ray spectral properties of 2S 0114+65 in quiescent states may have no significant differences from those in active states.

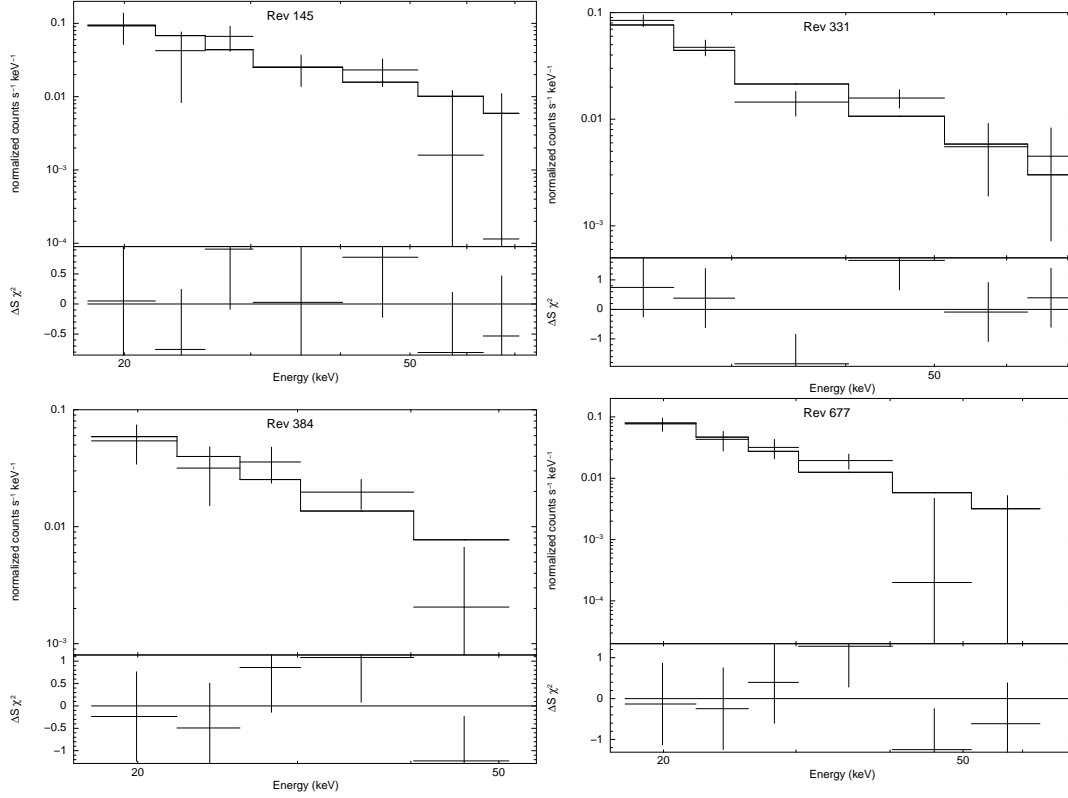


Figure 8. The hard X-ray spectrum of 2S 0114+65 obtained by INTEGRAL/IBIS during its quiescent states: Rev. 145, 331, 384, 677. In quiescence, the source cannot be detected significantly above ~ 50 keV. The spectra are fitted with a single pow-law model. See the text for details.

Table 3. INTEGRAL/JEM-X observations of 2S 0114+65 in 18 revolutions when the mean off-axis angle is below $\sim 5^\circ$ in Table 1. The source flux in the range of 3 – 35 keV in units of cts/s and detection significance level are also shown.

Rev. Num.	Flux	Detection significance
238	< 0.14	$< 5\sigma$
262	0.49 ± 0.11	5σ
263	0.42 ± 0.10	5σ
331	< 0.12	$< 5\sigma$
332	1.29 ± 0.06	24σ
333	0.61 ± 0.04	15σ
334	< 0.15	$< 5\sigma$
335	1.15 ± 0.07	16σ
454	< 0.12	$< 5\sigma$
528	< 0.14	$< 5\sigma$
664	1.65 ± 0.07	26σ
667	< 0.25	$< 5\sigma$
668	< 0.23	$< 5\sigma$
669	< 0.18	$< 5\sigma$
670	< 0.18	$< 5\sigma$
673	1.17 ± 0.06	20σ
675	0.79 ± 0.04	19σ
670	< 0.09	$< 5\sigma$

4.2 Hard X-ray tails

den Hartog et al. (2006) reported the detection of the high energy tail of 2S 0114+65 up to 120 keV without obvious high energy cutoff with the IBIS data, in which the spectrum was depicted by a combination of thermal bremsstrahlung and power-law models. This hard X-ray tail was also indicated in the spectrum of 2S 0114+65 during the time interval

of Rev 389 (see Fig. 7 & Table 2). We also check the IBIS data (Rev 142 – 148 & Rev 161 – 162) used by den Hartog et al. (2006). We also derived the hard X-ray spectra of the source for each revolution when 2S 0114+65 was bright. In Figure 9, we illustrate the spectra of 2S 0114+65 in two revolutions: 142 and 147.

In Rev 142, the source was detected with a significance level of $\sim 33\sigma$. The spectrum was fitted by a single power-law model of $\Gamma \sim 2.6 \pm 0.1$ (reduced $\chi^2 \sim 2.049$, 9d.o.f.) or a thermal bremsstrahlung model of $kT \sim 29.1 \pm 2.7$ keV (reduced $\chi^2 \sim 1.237$, 9d.o.f.). The data points above 80 keV cannot be fitted well. Thus we fit the spectrum using a thermal bremsstrahlung model plus a single power-law model, with $kT \sim 26.2 \pm 4.2$ keV and $\Gamma \sim 1.1 \pm 0.9$ (reduced $\chi^2 \sim 1.133$, 7d.o.f.). Then the high energy tail added in the model improved the fitting. The derived hard X-ray flux from 20 – 100 keV was $\sim (2.2 \pm 0.2) \times 10^{-10}$ erg cm $^{-2}$ s $^{-1}$.

The hard X-ray spectrum for Rev 147 was fitted with a single power-law model of $\Gamma \sim 2.7 \pm 0.2$ (reduced $\chi^2 \sim 1.476$, 8d.o.f.) or a thermal bremsstrahlung model of $kT \sim 22.1 \pm 4.1$ keV (reduced $\chi^2 \sim 1.687$, 8d.o.f.). The simple model also cannot fit the spectrum well. We then fit the spectrum using a thermal bremsstrahlung plus a single power-law model, with $kT \sim 17.9 \pm 3.1$ keV and $\Gamma \sim 0.7 \pm 0.9$ (reduced $\chi^2 \sim 0.899$, 6d.o.f.). The derived X-ray flux in the range of 20 – 100 keV was $(1.9 \pm 0.2) \times 10^{-10}$ erg cm $^{-2}$ s $^{-1}$.

Thus, we confirmed the hard X-ray tails reported by den Hartog et al. (2006) using the same datasets. We have detected the hard X-ray tails in 2S 0114+65 at least in two observational revolutions: 142, 147. Thus hard X-ray tails

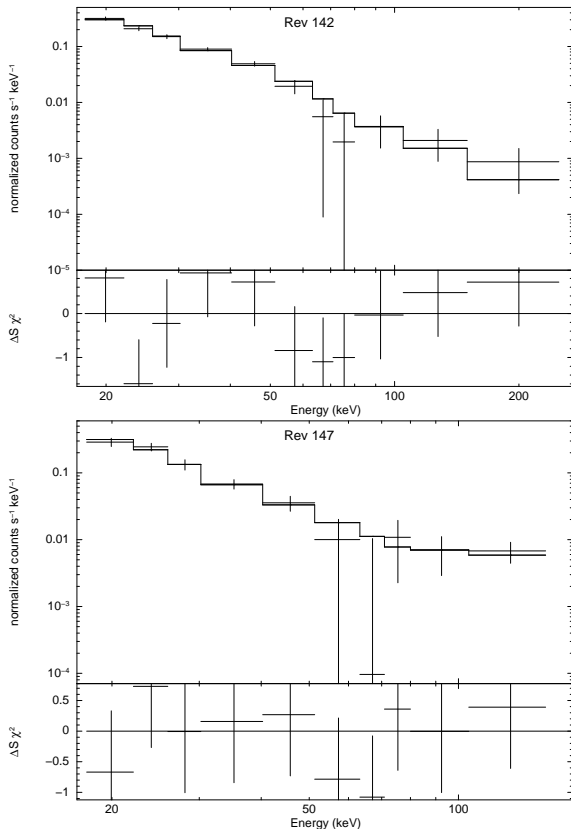


Figure 9. The hard X-ray spectra of 2S 0114+65 in two revolutions: 142 and 147. The hard X-ray tails above 70 keV are detected in the spectra. See the text for the details.

should really exist in such accretion neutron star systems. For neutron star X-ray binaries or accreting X-ray pulsars, their typical X-ray spectra from 1 keV to tens of keV can be generally described by an absorbed power-law model with a high energy exponential cut-off (Hall et al. 2000). Thus detection of this high energy tail is quite interesting for the accretion neutron star systems. The spectra of neutron star X-ray binaries generally have no hard X-ray tails which are different from those of black hole X-ray binaries. Then it is very important to investigate the characteristics and the origin of the hard X-ray tails in the neutron star accretion binary 2S 0114+65?

To constrain the hard X-ray tails in the spectra of 2S 0114+65, we will try to combine the soft X-ray band data in the range of 3 – 35 keV from JEM-X aboard INTEGRAL with the IBIS data above 18 keV. JEM-X has a small field of view so we can study 2S 0114+65 using JEM-X only when the mean off-axis angle on the source is below 5° . According to Table 1, only 18 revolutions meet the above detection condition. The JEM-X detection results on 2S 0114+65 for these 18 revolution are shown in Table 3. 2S 0114+65 was detected significantly by JEM-X (e.g., $> \sim 15\sigma$ in the energy band of 3 – 35 keV) in six revolutions. In Fig. 10, we plot the variations of source flux detected both by JEM-X and IBIS in the 18 revolutions. JEM-X can detect 2S 0114+65 when IBIS has very high detection significance level ($> 30\sigma$, except for Rev 673, $\sim 20\sigma$ for JEM-X and $\sim 17\sigma$ for IBIS).

We would try to study the combined spectral properties with JEM-X and IBIS, so we select the observational revolu-

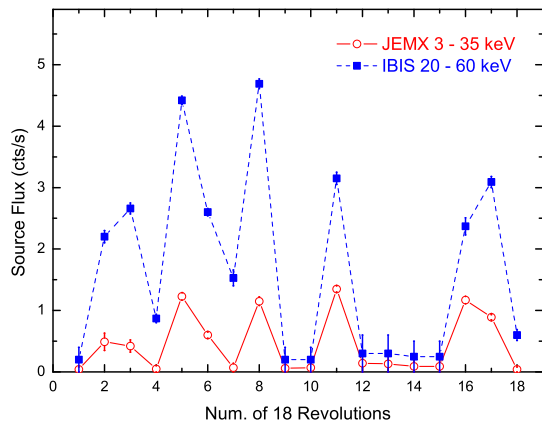


Figure 10. The JEM-X flux (3 – 35 keV) versus the IBIS/ISGRI flux (20 – 60 keV) for 2S 0114+65 in the 18 observational revolutions listed in Table 3.

tions when 2S 0114+65 was detected with significance level $> \sim 15\sigma$ both by JEM-X and IBIS. Six revolutions are used for the combined spectral analysis: Rev. 332, 333, 335, 664, 673 and 675 (see Table 3). The cross-calibration studies on the JEM-X and IBIS/ISGRI detectors have been done by Jourdain et al. (2008) using the Crab observation data. The calibration between JEM-X and IBIS/ISGRI for OSA 7.0 can be good enough within $\sim 6\%$. JEM-X only gave the upper limits for the weak source 2S 0114+65 above 20 keV in our observations, so we only use the spectral data points from 3 keV up to ~ 25 keV in the spectral analysis.

With the JEM-X data combined with the IBIS data, we can construct the X-ray spectrum from 3 – 100 keV even up to 200 keV for 2S 0114+65 to study the properties of the hard X-ray tail. In Fig. 11, we present the X-ray spectra from 3 – 100 keV (up to 200 keV in some cases) of 2S 0114+65 in six observational revolutions when both JEM-X and IBIS had the significant detections: Revs. 332, 333, 335, 664, 673 and 675. All the spectra are first fitted with an absorbed power-law model plus high energy exponential cutoff (hereafter *abs*pow*high*). In two Revs. 332 and 675, the high column densities ($\sim (6 - 7) \times 10^{22} \text{ cm}^{-2}$) are derived, and the *abs*pow*high* model fit the spectra well up to 120 keV, no hard X-ray tails are detected. In other Revs, spectral fittings with the *abs*pow*high* model imply a low column density (near zero in fittings or an upper limit of $\sim 3 \times 10^{22} \text{ cm}^{-2}$), so these spectra can be directly fitted by a power-law plus high energy exponential cutoff (hereafter *pow*high*). In three Revs. 333, 664 and 675, the significant flux excesses are detected above 70 keV, suggesting the existence of hard X-ray tails. In Rev 335, only one data point above 70 keV appears to be an excess, so we cannot conclude that it could be the hard X-ray tail.

From the spectral analysis in the energy band of 3 – 100 keV even up to 200 keV (see Fig. 11 and Table 4), the hard X-ray tails really exist in 2S 0114+65 for some time intervals. Our results confirmed den Hartog's studies, but most previous studies have not detected the hard X-ray tails. For comparison, we collected previous spectral measurements in

Table 4. Spectral properties and searching for hard X-ray tails in 2S 0114+65 from different observations or work. Most of the spectra were fitted by the model $abs*pow*high$, some of them by $pow*high$ or a single power-law model. The column density is in units of 10^{22} cm^{-2} , E_{cut} and E_{fold} in units of keV, flux in units of $10^{-10} \text{ erg cm}^{-2} \text{ s}^{-1}$ in the given energy range.

Work	Instrument	N_{H}	Γ	E_{cut}	E_{fold}	energy range (keV)	Flux	hard X-ray tail?
Hall et al. (2000)	RXTE	3.5 ± 0.3	1.37 ± 0.05	8.4 ± 0.4	20.3 ± 1.2	3 – 20	1.09	No
Bonning & Falanga (2005)	INTEGRAL	-	1.6	9	22.1	5 – 100	2.4	No
Masetti et al. (2006)	BeppoSAX	9.7 ± 0.9	1.33 ± 0.16	12 ± 3	21 ± 4	1.5 – 100	3.3	No
den Hartog et al. (2006)	INTEGRAL	-	3.1 ± 0.06	-	-	20 – 150	1.7	Yes
Farrell et al. (2008)	RXTE	3.2 ± 0.9	1.1 ± 0.1	6.0 ± 0.7	15 ± 3	3 – 50	2.3	No
This work								
Rev 332	INTEGRAL	6.9 ± 2.8	1.2 ± 0.1	6.1 ± 2.7	28.5 ± 3.2	3 – 100	6.4	No
Rev 333	INTEGRAL	-	0.9 ± 0.1	6.5 ± 2.1	20.5 ± 2.1	3 – 100	3.4	Yes
Rev 335	INTEGRAL	-	0.7 ± 0.1	5.9 ± 2.2	19.4 ± 1.7	3 – 100	5.9	?
Rev 664	INTEGRAL	-	0.7 ± 0.1	8.3 ± 0.5	8.4 ± 0.4	3 – 100	7.0	Yes
Rev 673	INTEGRAL	-	1.2 ± 0.2	7.7 ± 1.4	13.6 ± 1.7	3 – 100	4.9	Yes
Rev 675	INTEGRAL	6.5 ± 2.7	1.1 ± 0.2	6.9 ± 2.6	25.2 ± 3.9	3 – 100	4.6	No

Table 4. The work by Hall et al. (2000) and Farrell et al. (2008) used the data covering the energy range below 50 keV, so it is reasonable that they cannot detect the hard X-ray tails generally above 60 keV. Masetti et al. (2006) used the BeppoSAX data in the range of 1.5 – 100 keV, and did not detect the high energy tail but derived a large column density of $9.7 \times 10^{22} \text{ cm}^{-2}$. Their result is still consistent with our results: in two revolutions 332 and 675, no hard X-ray tails are detected with large column densities (see Table 4).

Therefore, we find that the detection of hard X-ray tails is sensitive to the column density. The hard X-ray tails are detected when the column density is very low (near zero in fittings). The high column density may lead to the disappearance of the hard X-ray tails. It is quite interesting because generally the large column density induces strong absorption in soft X-ray bands of 0.1 – 5 keV. Thus, our results may provide a clue to probe the origin of the hard X-ray tails in neutron star accretion systems, especially the relevant information for the physical environment.

4.3 Orbital phase-resolved spectral properties

The high mass X-ray binary 2S 0114+65 has an orbital period of ~ 11.59 day (Crampton et al. 1985; Corbet et al. 1999). The X-ray light curves of 2S 0114+65 shown in Fig. 2 cover about 3 orbital periods (12 continuous observational revolutions from Rev. 384 – Rev. 395 by IBIS/ISGRI). Then we try to derive the hard X-ray spectra for different orbital phases with the IBIS observational data from Rev. 384 – Rev. 395. To obtain the good detection significance for the spectral analysis in each orbital phase, we divide the orbital phase into four parts, and obtain the spectral properties for each orbital phase to show the spectral variations in different orbital phases. The phase-resolved data point starts from Rev. 384.

We derived four spectra of four different orbital phases (Figure 12). For a comparison, we used the same model to fit the continuum of all the spectra from 18 – 150 keV: a power-law model with a high energy exponential cutoff. We also compare variations of the three spectral parameters over orbital phases: photon index Γ , the cutoff energy E_{cut} and the e-folding energy E_{fold} for four orbital phases.

The hard X-ray spectral parameters of 2S 0114+65 in the different orbital phases were presented together for comparison in Table 5. In phase 1, the photon index was $\Gamma \sim 2.56 \pm 0.41$, and $E_{\text{cut}} \sim 10.8 \pm 2.1$ keV with $E_{\text{fold}} \sim 19.3 \pm 4.2$ keV (reduced $\chi^2 \sim 0.968$, 6d.o.f.), and above 60 keV, 2S 0114+65 can not be detected significantly during phase 1. In phase 2, $\Gamma \sim 1.53 \pm 0.35$, $E_{\text{cut}} \sim 18.9 \pm 1.6$ keV with $E_{\text{fold}} \sim 27.4 \pm 4.8$ keV (reduced $\chi^2 \sim 0.717$, 7d.o.f.); in phase 3, $\Gamma \sim 1.92 \pm 0.31$, $E_{\text{cut}} \sim 25.8 \pm 1.3$ keV with $E_{\text{fold}} \sim 35.9 \pm 3.1$ keV (reduced $\chi^2 \sim 0.799$, 7d.o.f.); and in phase 4, $\Gamma \sim 2.18 \pm 0.38$, and the high energy cutoff given as $E_{\text{cut}} \sim 24.0 \pm 2.1$ keV with $E_{\text{fold}} \sim 69.8 \pm 10.2$ keV (reduced $\chi^2 \sim 1.18$, 7d.o.f.).

From the continuum fits, we found that the spectral properties of 2S 0114+65 changed with the orbital phases. In Figure 13, we plot the changes of the three fitted parameters: Γ , E_{cut} and E_{fold} with the orbital phases. The changes of the photon index and E_{cut} looks like a sinusoidal curve: at the maximum of the light curve, the spectrum is harder with smaller photon index with a larger high energy cut-off. The variation of the power-law photon index over orbital phase anticorrelates with hard X-ray flux, and the variation of E_{cut} has a positive correlation with the hard X-ray flux. Farrell et al. (2008) found that the variations of neutral hydrogen column density and power-law photon index also have anticorrelations with the X-ray flux using the RXTE/PCA 2 – 9 keV data. At the minimum of the light curve, the increase of the column density and photon index suggested the presence of the strong absorption effect by the dense stellar wind. Thus, the change of the hard X-ray properties in 2S 0114+65 over orbital phase is still consistent with those in soft X-ray bands.

In addition, we also tried to search for the possible cyclotron absorption features after the continuum fittings of the four spectra (see the residuals in Figure 12). However, no significant absorption features were detected in all orbital phase-resolved spectra.

5 SUMMARY AND DISCUSSION

In this paper, we have carried out the long-term hard X-ray monitoring of the high mass X-ray binary 2S 0114+65 with the soft gamma-ray detector IBIS/ISGRI aboard IN-

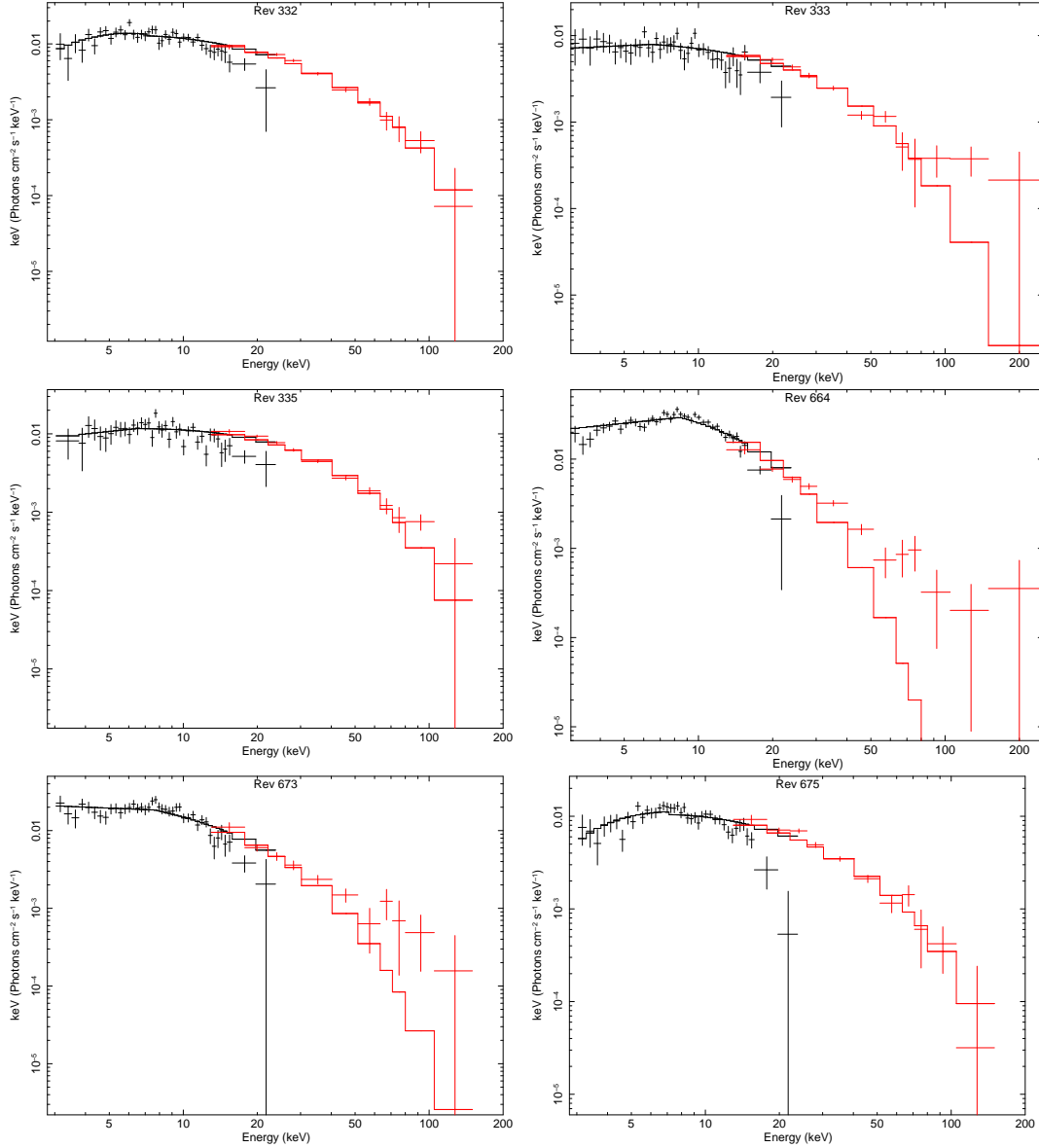


Figure 11. The unfolded hard X-ray spectra from 3 – 100 keV of 2S 0114+65 with the combined observational data of IBIS and JEM-X in six time intervals: Revs. 332, 333, 335, 664, 673 and 675.

Table 5. Hard X-ray spectral properties of 2S 0114+65 in different orbital phases. All spectra are fitted by the pow*high model.

Phase	Γ	E_{cut} (keV)	E_{fold} (keV)
0.0 – 0.25	2.56 ± 0.41	10.8 ± 2.1	19.3 ± 4.2
0.25 – 0.5	1.53 ± 0.35	18.9 ± 1.6	27.4 ± 4.8
0.5 – 0.75	1.92 ± 0.31	25.8 ± 1.3	35.9 ± 3.1
0.75 – 1.0	2.18 ± 0.38	24.0 ± 2.1	69.8 ± 10.2

TEGRAL. 2S 0114+65 is a variable X-ray source whose luminosity changes with the orbital phase. The hard X-ray properties changed in different accretion states and over the orbital phases. The characteristics of the spin period of the neutron star in 2S 0114+65, the variations of hard X-ray properties over orbital phases and conspicuous features of the hard X-ray tails are investigated in detail.

The main results from our hard X-ray monitoring project on 2S 0114+65 are presented as follows:

- (1) The spin evolution of the neutron star in 2S 0114+65 is studied. With the observations covering near five years from 2003 December to 2008 May, we obtained the values of the spin period of the neutron star in 2S 0114+65 in six time intervals when 2S 0114+65 was detected with a high significance level: 2003 Dec, $P = 9612 \pm 20$ s ; 2004 Feb, $P = 9600 \pm 20$ s ; 2004 Dec, $P = 9570 \pm 20$ s ; 2005 July, $P = 9555 \pm 15$ s ; 2005 Dec – 2006 Jan, $P = 9520 \pm 20$ s ; 2008 April $P = 9475 \pm 25$ s. Thus we obtained a spin-up rate of the neutron star in 2S 0114+65 $\sim 1.09 \times 10^{-6}$ s s $^{-1}$ from 2003 – 2008. Compared with the previous reported spin-up rate, the neutron star in 2S 0114+65 was spinning up, and the spin-up rate was accelerating.
- (2) Hard X-ray spectral properties of 2S 0114+65 changed in different time intervals and accretion states (see Figs. 7

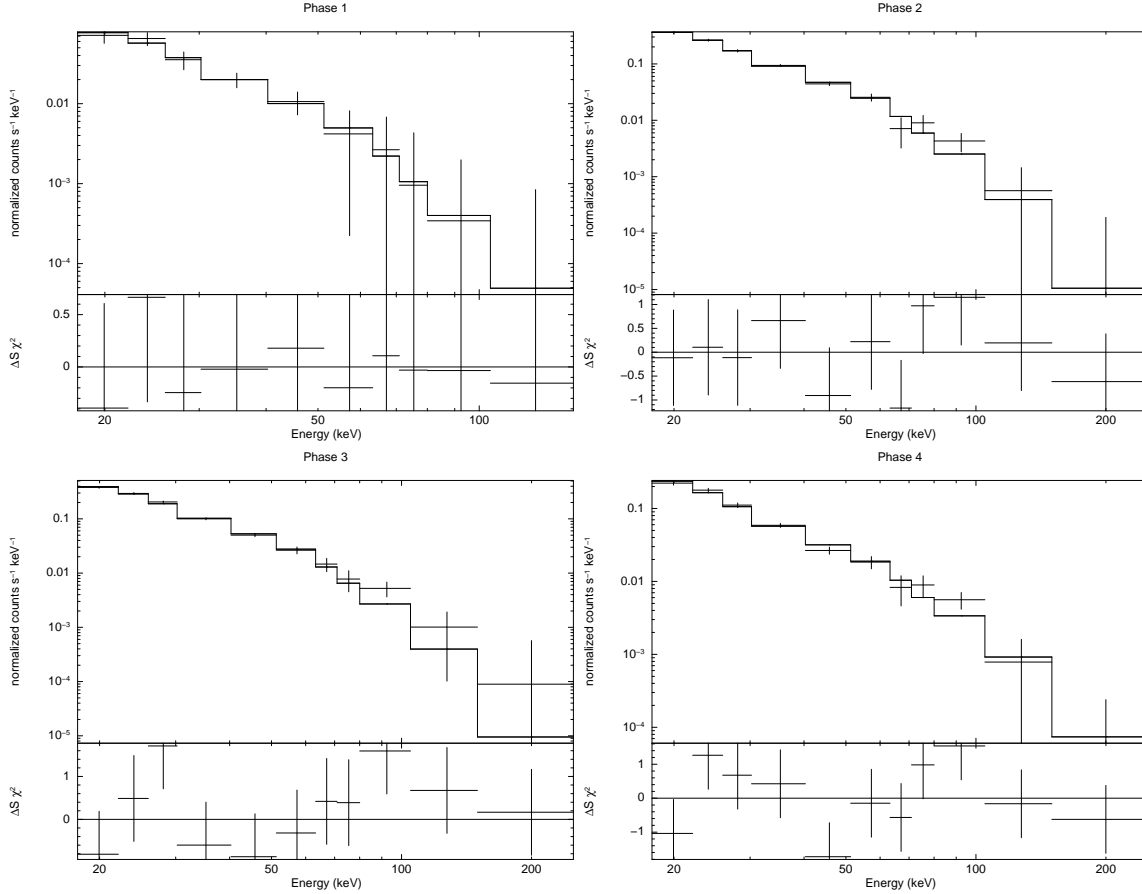


Figure 12. The hard X-ray spectra of 2S 0114+65 in four orbital phases: phase 1 (0.0–0.25); phase 2 (0.25 – 0.5); phase 3 (0.5–0.75); and phase 4 (0.75 – 1.0). For a comparison, all spectra are fitted with the same spectral model: a power-law model with a high energy cutoff. See details in the text.

& 8). The detected hard X-ray luminosity from 20 – 100 keV varies from 10^{35} erg to 4×10^{36} erg. For the comparison, the spectra of 2S 0114+65 in different states are fitted with the same spectral model – a single power-law model. In active states, the photon index varies from 2.5 – 2.8; in quiescent states, 2S 0114+65 was not detected significantly above 50 keV with $\Gamma \sim 2.6 - 3.2$. The cyclotron absorption line features at 22 keV and 44 keV cannot be confirmed by our spectral studies.

(3) Hard X-ray tails above 60 keV are detected in the spectra of 2S 0114+65 in some revolutions. The 20 – 120 keV spectra can be fitted by the bremsstrahlung model plus a power-law (see Fig. 9). We also obtained the broadband spectra from 3 – 100 keV using both JEM-X and IBIS data to constrain the continuum spectral properties and study the characteristics of hard X-ray tails. The 3 – 100 keV can generally be described by an absorbed power-law model with high energy cutoff. When the derived values of column density are higher than $\sim 3 \times 10^{22} \text{ cm}^{-2}$, no hard X-ray tails are detected. While in the case of low column density (column density is near zero in our fittings), hard X-ray tails are detected. The flux excesses above 60 keV cannot be fitted with the model $abs*pow*highE$. Therefore, detections of hard X-ray tails are sensitive to the column density. High column density may lead to the disappearance of the hard X-ray tails in the spectra of 2S 0114+65. Our results confirm the

den Hartog’s report on hard X-ray tail in 2S 0114+65, and can also reasonably explain why previous studies did not detect high energy tails (see Table 4). Though the origin of hard X-ray tails in neutron star accretion systems such as 2S 0114+65 is unclear, our results would provide a good clue to probe the origin.

(4) Finally, we also study the variations of spectral properties of 2S 0114+65 with different orbital phases. All hard X-ray spectra from 20 – 150 keV were fitted with a power-law model with a high energy cutoff. The variation of the power-law photon index over orbital phase anticorrelates with hard X-ray flux, and the variation of E_{cut} has a positive correlation with the hard X-ray flux, suggesting that the harder spectrum at the maximum of the light curve. The variations of spectral properties of 2S 0114+65 over orbital phase are consistent with the feature in the highly obscured binary system. The possible cyclotron absorption features around 22 keV and 44 keV were not detected in all orbital phase-resolved spectra.

The possible electron cyclotron resonant scattering features (CRSF) around 22 keV (Bonning & Falanga 2005) was not detected in our long-term INTEGRAL/IBIS observations. The CRSF around 22 keV was also not detected by other independent observations (Masetti et al. 2006; den Hartog et al. 2006; Farrell et al. 2008). The possible absorption feature at ~ 44 keV was also not evident in our spectra

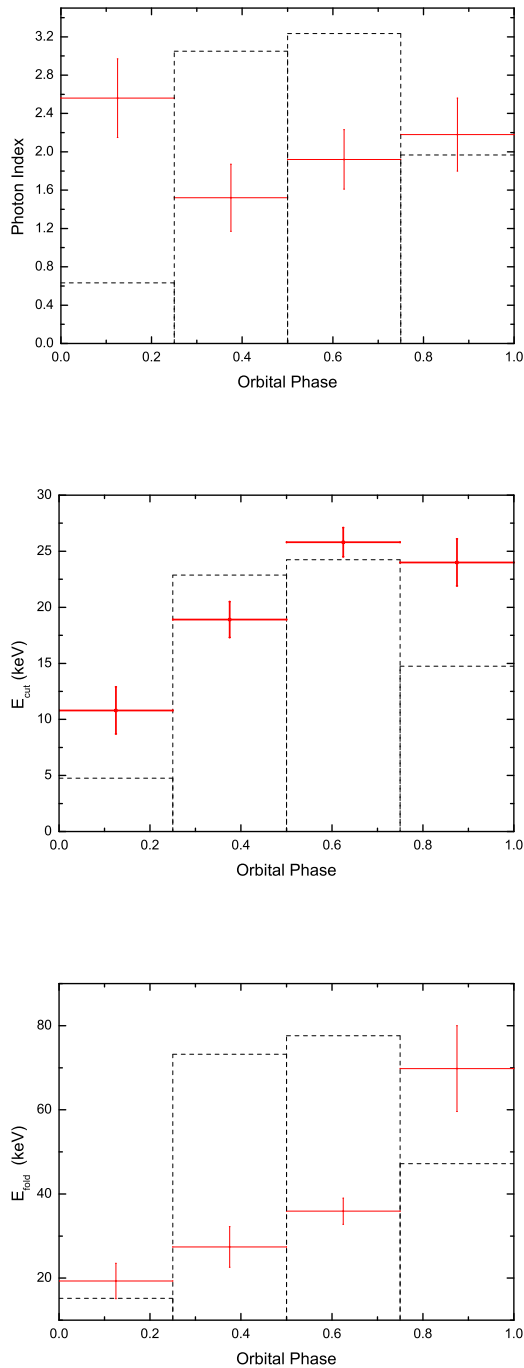


Figure 13. The spectral properties of 2S 0114+65 with the different orbital phases. For four spectra of four orbital phases, we use the power-law model with a high energy cutoff to fit the continuum of all the spectra. And we show the fitted parameters: the photon index (top), the high cutoff energy (E_{cut} , middle) and the exponential folding energy (E_{fold} , bottom) over four orbital phases. The orbital variability of the normalized flux rates in hard X-ray bands is also plotted (dashed curves) for a comparison

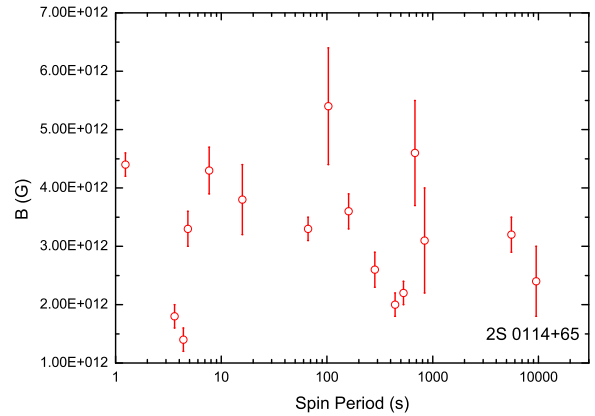


Figure 14. Magnetic field of X-ray accretion pulsars from measurements of cyclotron resonant absorption features. Spin period of the neutron stars are also shown. For 2S 0114+65, the possible value of magnetic field are displayed by assuming 22 keV (Bonning & Falanga 2005) as the fundamental line energy. The other points are collected from Coburn et al. (2002), Kreykenbohm et al. (2005), McBride et al. (2006), and Wang (2009).

but was only hinted in one observational revolution in active states. In theories, the scattering cross-section is dependent on the angle between photon direction and the magnetic field (Schoenherr et al. 2007), so CRSFs provide a diagnostic of the emission geometry and the physical conditions of the radiating plasma (Harding & Lai 2006). For example, when the photon direction and magnetic field vector are aligned, no CRSFs are expected. Variations in the CRSFs are also expected with the viewing geometry, accretion geometry or electron density and even the accretion rate (see Araya & Harding 1999, 2000). The relativistic cyclotron absorption line energy would have non-harmonic line spacing and changed with luminosity and some relevant parameters (Araya & Harding 1999; Klochkov et al. 2008). Thus possible CRSFs are not excluded. If we assume the 22 keV line as the fundamental, the magnetized neutron star with the magnetic field of $\sim 2.5 \times 10^{12}$ G is harboured in 2S 0114+65 which is preferred by the formation scenario proposed by Li & van den Heuvel (1999). Up to now, the cyclotron absorption line features are detected in more than 10 high mass X-ray binary systems. The energy of the fundamental line distributes from 10 – 50 keV, corresponding to a magnetic field of $\sim (1.6 - 6) \times 10^{12}$ G (see Figure 14). In Figure 13, we show the magnetic field of neutron stars derived from the electron cyclotron absorption line measurements versus their spin periods in accretion X-ray binaries up to now; for 2S 0114+65, the possible CRSF at 22 keV is taken. We found that the magnetic field has no correlation to the spin period of the neutron stars in high mass X-ray binaries.

We have studied the hard X-ray spectral properties of 2S 0114+65 in different accretion states. The change of the spectral properties of 2S 0114+65 with the orbital phase in hard X-rays (18 – 150 keV) were presented. In soft X-rays (e.g., 2 – 9 keV), the spectral properties also changed with the orbital phases as suggested by the RXTE/PCA observations (Farrell et al. 2008). In soft X-ray bands, the

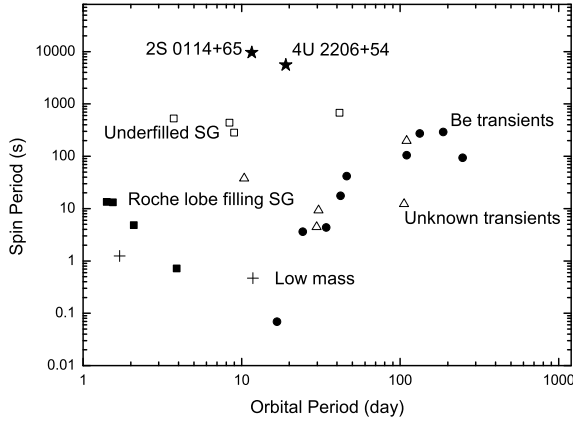


Figure 15. The spin period - orbital period diagram for the accreting neutron star systems (the Corbet diagram, Corbet 1986). The data point for 2S 0114+65 is taken from this work and Farrell et al. (2008); the data point for 4U 2206+54 is taken from Wang (2009); other points are taken from Bildsten et al. (1997). There exist a positive correlation between $P_{\text{spin}} - P_{\text{orbit}}$ for the Be transient systems; and a possible negative correlation for the disk-accretion system including Roche Lobe Filling Supergiants and low mass systems; For the underfilled Roche Lobe Supergiants and two long-pulsation systems 2S 0014+65, 4U 2206+54 which all belong to wind-fed accretion systems, the possible relation between $P_{\text{spin}} - P_{\text{orbit}}$ is different from that of the Be transients.

observed variability of the neutral hydrogen column density over the orbital period indicated that the variable absorption by the dense stellar wind medium is the mechanism behind the orbital modulation (Farrell et al. 2008). The variability of fitted photon index from 2 – 9 keV against orbital phase showed a good anti-correlation between the photon index and count rate, implying a harder spectrum around the maximum of the count. In hard X-ray bands, the variability of photon index over orbital phase has an anticorrelation with the flux. In addition, we also derived the variation of high energy cut-off over orbital phase which has a positive correlation with the flux. Thus around the maximum of the count rate the spectrum appeared harder, which is similar to the case in soft X-rays.

The high energy tails in the spectra of 2S 0114+65 above 70 keV are detected and studied in details using the IBIS data combined with JEM-X observations. High column density would lead to disappearance of hard X-ray tails. The hard X-ray tails in X-ray binaries have been reported in black hole accretion systems and low-mass X-ray binaries. How to produce the hard X-ray tails above 70 keV for accreting neutron star in high mass X-ray binaries especially in the wind-fed accretion systems is unclear. Generally, hard X-ray tails are suggested to be linked to three possible scenarios: compact jets, accretion disc or hot corona. The results from radio observations of 2S 0114+65 (Farrell et al. 2007) are against the possibility of the presence of jets. In addition, the stable accretion disc seems to be impossible to form in stellar-wind accretion systems like 2S 0114+65, but the transient accretion disc is still possible (Crampton et al. 1985). Hot corona with temperature of $kT > 10$ keV

around inner part of stable accretion disc is suggested in X-ray black hole binary systems. Formation of hot corona is not so clear yet but it may be related to outflows from accretion compact objects. So it is possible that hot corona exists near neutron stars for wind-fed accretion systems like 2S 0114+65. The formation of the corona and production processes of hard X-ray tails are beyond the scope of this paper. Moreover, from our observations, the dense accretion materials or strong winds prevent the formation of hot corona or depress the comptonization effects. In summary, hard X-ray tails in accretion neutron star systems like 2S 0114+65 is interesting for both theorists and observers, requiring future work on both theories and observations.

2S 0114+65 is one of the slowest pulsation neutron star systems. In the $P_{\text{spin}} - P_{\text{orbit}}$ diagram (see Fig. 15), 2S 0114+65 and the other super-slow pulsation neutron star binary 4U 2206+54 ($P_{\text{spin}} \sim 1.57$ hr, $P_{\text{orb}} \sim 19.12$ days, see Corbet et al. 2007; Reig et al. 2009; Wang 2009) have the similar properties to underfilled Roche Lobe Supergiants which are also powered by direct wind accretion. These systems may follow a $P_{\text{spin}} - P_{\text{orbit}}$ relation quite different from that of the Be transient systems (Fig. 15). 2S 0114+65 and 4U 2206+54 are the only two known super-slow pulsation neutron star high mass X-ray binaries ($P_{\text{spin}} > 1000$ s), and two possible super-slow X-ray pulsar candidates were also reported recently: 1E 161348-5055 in a young supernova remnant RCW 103 ($P_{\text{spin}} \sim 6.67$ hr, De Luca et al. 2006), and a wind-accretion symbiotic low mass X-ray binary 4U 1954+319 ($P_{\text{spin}} \sim 5$ hr, Mattana et al. 2006). The formation mechanisms of these super-slow X-ray pulsars are unclear. Li & van den Heuvel (1999) have studied the origin of the long pulsation period X-ray pulsars and suggested that a slow period is possible if the neutron star was born as a magnetar with an initial magnetic field $\geq 10^{14}$ G, decaying to a current value of 10^{12} G, allowing the neutron star to spin down to the measured spin period within the lifetime (Myr) of the companion. An alternative formation channel proposed by Ikhshanov (2007) showed that an initial magnetic field strength of $B \gg 10^{13}$ G is not necessary if the evolutionary sequence of the neutron star consisted of both supersonic and subsonic propeller phases. Anyway, both scenarios predicted that the equilibrium period for 2S 0114+65 would be less than 26 min, and this spin period will be approached on time scales of < 100 yr for disc accretion and < 1000 yr for stellar wind accretion (Ikhshanov 2007). From our measurements, the spin-up rate of 2S 0114+65 at present is around 1.1×10^{-6} s s^{-1} , and the spin-up rate was still accelerating in the last 30 years. If 2S 0114+65 would still spin up in the future, the pulsar in 2S 0114+65 would reach its equilibrium period less than 200 years. The very short time scale suggested that the long pulsation period X-ray pulsars should be very rare. Presently it is fortunate (maybe strange from the probability of detection) that at least three candidates are discovered. However, it is still possible that 2S 0114+65 and other super-slow X-ray pulsars are still young systems. Thus the current understanding of the pulsar formation in different systems is quite deficient. Further theoretic work may be required. It is hoped that future observations of the spin-period evolution of 2S 0114+65 and other similar systems would help us to understand the formation mechanism of the long spin period.

ACKNOWLEDGMENTS

We are very grateful to the referee's fruitful comments and suggestions to improve the paper. This paper is based on observations of INTEGRAL, an ESA project with instrument and science data centre funded by ESA member states (principle investigator countries: Denmark, France, Germany, Italy, Switzerland and Spain), the Czech Republic and Poland, and with participation of Russia and US. W. Wang is supported by the National Natural Science Foundation of China under grants 10803009, 10833003, 11073030.

REFERENCES

- Aab, O.E., Bychkova, L.V., Kopylov, I.M. 1983, *Sov. Astron. Lett.*, 9, 285
- Araya, R.A. & Harding, A.K. 1999, *ApJ*, 517, 334
- Araya, R.A. & Harding, A.K. 2000, *ApJ*, 544, 1067
- Bildsten, L. et al. 1997, *ApJS*, 113, 367
- Bird, A.J. et al., 2007, *ApJS*, 170, 175
- Bonning, E.W. & Falanga, M. 2005, *A&A*, 436, L31
- Coburn, W. et al. 2002, *ApJ*, 580, 394
- Corbet, R.H.D., 1986, *MNRAS*, 220, 1047
- Corbet, R.H.D., Finley, J.P., Peele, A.G., 1999, *ApJ*, 511, 876
- Corbet, R.H.D., Markwardt, C.B. & Tueller, J., 2007, *ApJ*, 655, 458
- Crampton, D., Hutchings, J.B., Cowley, A.P., 1985, *ApJ*, 299, 839
- den Hartog et al. 2006, *A&A*, 451, 587
- De Luca, A. et al. 2006, *Science*, 313, 814
- Farrell, S.A. et al. 2006, *MNRAS*, 367, 1457
- Farrell, S.A. et al. 2007, in Antonelli L. A. et al. eds, *AIP Conf. Proc. Vol. 924, The Multi-coloured Landscape of Compact Objects and their Explosive Origins*. AIP, Melville, p. 885
- Farrell, S.A. et al. 2008, *MNRAS*, 389, 608
- Finley, J.P., Belloni, T., Cassinelli, J.P., 1992, *A&A*, 262, L25
- Goldwurm, A. et al., 2003, *A&A*, 411, L223
- Grundstom, E.D. et al. 2007, *ApJ*, 656, 431
- Hall, T.A. et al. 2000, *ApJ*, 536, 450
- Harding, A.K. & Lai, D. 2006, *Rep. Prog. Phys.*, 69, 263
- Ikhsanov, N.R. 2007, *MNRAS*, 375, 698
- Jourdain, E. et al. 2008, *POS INTEGRAL08*, 144 (arXiv:0810.0646)
- Klochkov, D. et al. 2008, *A&A*, 482, 907
- Kreykenbohm, I. et al., 2005, *A&A*, 433, L45
- Lebrun, F. et al., 2003, *A&A*, 411, L141
- Li, X.D. & van den Heuvel, E.P.J., 1999, *ApJ*, 513, L45
- Lund, N. et al., 2003, *A&A*, 411, L231
- Masetti, N. et al., 2006, *A&A*, 445, 653
- Mas-Hesse, J.M. et al. 2003, *A&A*, 411, L261
- Mattana, F. et al. 2006, *A&A*, 460, L1
- McBride V. A. et al. 2006, *A&A*, 451, 267
- Reig, P. et al. 1996, *A&A*, 311, 879
- Reig, P. et al., 2009, *A&A*, 494, 1073
- Schoenherr G. et al. 2007, *A&A*, 472, 353
- Ubertini, P. et al., 2003, *A&A*, 411, L131
- Vedrenne, G. et al., 2003, *A&A*, 411, L63
- Wang, W. 2009, *MNRAS*, 398, 1428
- Wen, L. et al. 2006, *ApJS*, 163, 372
- Winkler, C. et al. 2003, *A&A*, 411, L1

Table 1. Spectral properties of 2S 0114+65 in different accretion states and datasets (for observations in each revolution).

Rev. Num.	Model	Γ / kT (keV)	E_{cut} (keV)	E_{fold} (keV)	Flux (10^{-10} erg cm $^{-2}$ s $^{-1}$)	reduced χ^2
The active states						
142	power	2.6 ± 0.1	-	-	2.9 ± 0.2	2.049(9d.o.f.)
	bremss	29.1 ± 2.7	-	-	2.2 ± 0.2	1.237(9d.o.f.)
	bremss+power	$1.1 \pm 0.9/26.2 \pm 4.2$	-	-	2.2 ± 0.2	1.133(7d.o.f.)
161	power	2.8 ± 0.1	-	-	2.3 ± 0.4	1.252(25d.o.f.)
	bremss	22.8 ± 1.6	-	-	2.1 ± 0.4	0.791(25d.o.f.)
	pow*high	2.0 ± 0.8	24.1 ± 8.2	33.0 ± 16.9	2.1 ± 0.4	0.810(23d.o.f.)
262	power	2.6 ± 0.2	-	-	1.6 ± 0.3	0.847(26d.o.f.)
	bremss	27.9 ± 3.9	-	-	1.5 ± 0.3	0.704(26d.o.f.)
	pow*high	1.7 ± 1.1	22.4 ± 11.7	35.7 ± 30.8	1.5 ± 0.3	0.759(24d.o.f.)
263	power	2.7 ± 0.1	-	-	1.9 ± 0.3	1.177(26d.o.f.)
	bremss	26.8 ± 2.3	-	-	1.7 ± 0.3	1.288(26d.o.f.)
	pow*high	2.1 ± 0.9	23.3 ± 17.1	50.7 ± 45.8	1.8 ± 0.3	1.244(24d.o.f.)
264	pow	2.7 ± 0.1	-	-	2.5 ± 0.4	0.793(24d.o.f.)
	bremss	26.5 ± 2.5	-	-	2.4 ± 0.4	0.705(24d.o.f.)
	pow*high	1.7 ± 0.7	15.2 ± 14.5	33.4 ± 21.6	2.4 ± 0.4	0.729(22d.o.f.)
265	pow	2.6 ± 0.1	-	-	3.9 ± 0.3	1.253(27d.o.f.)
	bremss	26.8 ± 1.5	-	-	3.6 ± 0.3	0.975(27d.o.f.)
	pow*high	2.1 ± 0.3	27.4 ± 6.5	50.0 ± 16.0	3.7 ± 0.3	0.899(25d.o.f.)
332	power	2.5 ± 0.1	-	-	3.0 ± 0.2	5.711(9d.o.f.)
	bremss	28.1 ± 1.2	-	-	2.9 ± 0.3	1.216(9d.o.f.)
	pow*high	1.6 ± 0.4	20.3 ± 4.1	30.9 ± 9.8	2.9 ± 0.3	0.932(7d.o.f.)
333	power	2.5 ± 0.1	-	-	1.8 ± 0.2	2.697(10d.o.f.)
	bremss	28.1 ± 1.9	-	-	1.7 ± 0.3	1.764(10d.o.f.)
	bremss+power	$0.7 \pm 0.9/20.0 \pm 4.5$	-	-	1.7 ± 0.3	0.932(8d.o.f.)
335	power	2.6 ± 0.1	-	-	3.3 ± 0.3	4.172(10d.o.f.)
	bremss	30.4 ± 1.4	-	-	3.2 ± 0.3	0.762(10d.o.f.)
	pow*high	1.7 ± 0.3	21.7 ± 4.9	40.7 ± 11.2	3.2 ± 0.3	0.677(8d.o.f.)
385	power	2.7 ± 0.1	-	-	2.6 ± 0.3	0.973(27d.o.f.)
	bremss	26.2 ± 2.1	-	-	2.5 ± 0.3	0.798(27d.o.f.)
	pow*high	1.4 ± 0.6	13.6 ± 15.5	27.1 ± 12.3	2.5 ± 0.3	0.858(25d.o.f.)
386	power	2.6 ± 0.1	-	-	4.1 ± 0.3	1.490(29d.o.f.)
	bremss	28.3 ± 1.5	-	-	3.9 ± 0.3	0.826(29d.o.f.)
	pow*high	1.6 ± 0.5	19.0 ± 5.1	30.6 ± 10.5	3.9 ± 0.3	0.856(27d.o.f.)
389	power	2.8 ± 0.1	-	-	2.4 ± 0.3	1.052(29d.o.f.)
	bremss	24.2 ± 1.9	-	-	2.2 ± 0.3	1.059(29d.o.f.)
	bremss+power	$1.2 \pm 1.9/18.6 \pm 5.5$	-	-	2.3 ± 0.3	0.911(27d.o.f.)
395	power	2.6 ± 0.1	-	-	2.4 ± 0.3	0.986(29d.o.f.)
	bremss	30.4 ± 3.0	-	-	2.3 ± 0.3	0.951(29d.o.f.)
	pow*high	1.9 ± 0.6	18.0 ± 11.2	50.7 ± 31.8	2.3 ± 0.3	0.977(27d.o.f.)
664	power	2.8 ± 0.1	-	-	2.4 ± 0.3	1.321(10d.o.f.)
	bremss	22.1 ± 1.7	-	-	2.1 ± 0.3	1.089(10d.o.f.)
	bremss+power	$0.9 \pm 1.3/19.2 \pm 4.1$	-	-	2.2 ± 0.3	0.909(8d.o.f.)
675	power	2.7 ± 0.1	-	-	2.6 ± 0.3	1.580(10d.o.f.)
	bremss	24.5 ± 1.6	-	-	2.4 ± 0.3	0.922(10d.o.f.)
	pow*high	1.8 ± 0.4	11.8 ± 12.5	35.9 ± 15.8	2.5 ± 0.3	0.916(8d.o.f.)
The quiescent states						
145	power	2.7 ± 0.6	-	-	0.47 ± 0.11	0.689(5d.o.f.)
	bremss	38.9 ± 25.8	-	-	0.43 ± 0.11	0.577(5d.o.f.)
331	power	3.1 ± 0.3	-	-	0.51 ± 0.09	1.52(4d.o.f.)
	bremss	13.6 ± 10.4	-	-	0.47 ± 0.09	2.529(4d.o.f.)
384	power	2.6 ± 0.7	-	-	0.19 ± 0.07	1.21(3d.o.f.)
	bremss	33.3 ± 11.5	-	-	0.19 ± 0.07	1.02(3d.o.f.)
677	power	3.2 ± 0.6	-	-	0.29 ± 0.09	0.953(4d.o.f.)
	bremss	15.3 ± 5.5	-	-	0.29 ± 0.09	0.755(4d.o.f.)

In the **Appendix**, we show an extended table (compared with Table 2 in the paper) to present the spectral fittings with different models, like a single power law model *power*, a thermal bremsstrahlung model *bremss*, a power-law plus exponential high energy cutoff *pow*high*. For some revolutions, the spectra show the possible high energy tails, we would fit the spectra with the combined model: the bremsstrahlung plus a power-law model. Here we just display the spectral parameters for each revolution with different model fittings, let the readers independently justify which model would be more acceptable to fit the spectrum of 2S 0114+65 in different accretion states. The hard X-ray fluxes in the range of 20 – 100 keV for the active states and 20 – 50 keV for quiescent states in different fits are presented.